ACSNANO
www.acsnano.org
ARTICLE

Complex Magnetic Exchange Coupling between Co Nanostructures and Ni(111) across Epitaxial Graphene

Alessandro Barla,[*,†] Valerio Bellini,[‡] Stefano Rusponi,[¶] Paolo Ferriani,[§] Marina Pivetta,[¶] Fabio Donati,[¶] François Patthey,[¶] Luca Persichetti,[∥] Sanjoy K. Mahatha,[†] Marco Papagno,[#] Cinthia Piamonteze,[▽] Simon Fichtner,[§] Stefan Heinze,[§] Pietro Gambardella,[∥] Harald Brune,[¶] and Carlo Carbone[†]

[†]Istituto di Struttura della Materia (ISM), Consiglio Nazionale delle Ricerche (CNR), I-34149 Trieste, Italy
[‡]S3-Istituto di Nanoscienze-CNR, Via Campi 213/A, I-41125 Modena, Italy
[¶]Institute of Condensed Matter Physics (ICMP), Ecole Polytechnique Fédérale de Lausanne (EPFL), Station 3, CH-1015 Lausanne, Switzerland
[§]Institute of Theoretical Physics and Astrophysics, University of Kiel, D-24098 Kiel, Germany
[∥]Department of Materials, ETH Zurich, CH-8093 Zurich, Switzerland
[#]Dipartimento di Fisica, Università della Calabria, I-87036 Arcavacata di Rende (Cs), Italy
[▽]Swiss Light Source, Paul Scherrer Institut, CH-5232 Villigen PSI, Switzerland

Supporting Information

ABSTRACT: **We report on the magnetic coupling between isolated Co atoms as well as small Co islands and Ni(111) mediated by an epitaxial graphene layer. X-ray magnetic circular dichroism and scanning tunneling microscopy combined with density functional theory calculations reveal that Co atoms occupy two distinct adsorption sites, with different magnetic coupling to the underlying Ni(111) surface. We further report a transition from an antiferromagnetic to a ferromagnetic coupling with increasing Co cluster size. Our results highlight the extreme sensitivity of the exchange interaction mediated by graphene to the adsorption site and to the in-plane coordination of the magnetic atoms.**

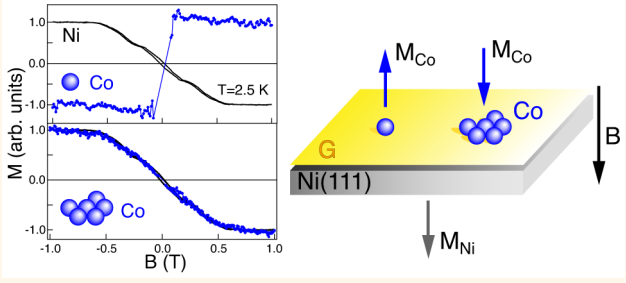

KEYWORDS: *magnetic exchange interaction, graphene, X-ray magnetic circular dichroism (XMCD), scanning tunneling microscopy (STM), density functional theory (DFT)*

Graphene is attracting a lot of interest as material for carbon-based nanoelectronics, due to its extraordinary in-plane charge carrier mobility,[1,2] combined with a low spin−orbit interaction, ideal for planar spin transport.[3−7] The weak van der Waals interaction of graphene with other materials[8,9] makes it an ideal spacer preserving the electronic properties of adjacent layers.

In order to access the potential of graphene in spintronic devices, its ability to mediate magnetic exchange interactions has to be assessed. It was shown that graphene and graphite films sandwiched between ferromagnetic layers exhibit sizable tunnel magnetoresistance.[10−13] Exchange coupling with a magnetic substrate across a graphene spacer has been investigated in molecular spin systems. Both ferro- and antiferromagnetic (FM and AFM) couplings of the order of few millielectronvolts have been observed depending on the choice of the molecule.[14−18] A more direct assessment of the TM-G-TM (TM = transition-metal, G = graphene) exchange coupling is obtained by replacing molecules with individual TM atoms, clusters, or monolayers. This choice also enables the study of the dependence of the exchange interaction on the size of magnetic centers. This is of the utmost importance as nanotechnologies are currently moving from thin layers to isolated nanostructures, whose dimensionality generally strongly influences their magnetic properties.[19−24]

Here we present the first direct evidence of significant magnetic exchange coupling between Co and Ni across a graphene layer. Our investigations, based on X-ray magnetic

Received: October 12, 2015
Accepted: November 20, 2015
Published: November 20, 2015

DOI: 10.1021/acsnano.5b06410
ACS Nano 2016, 10, 1101−1107

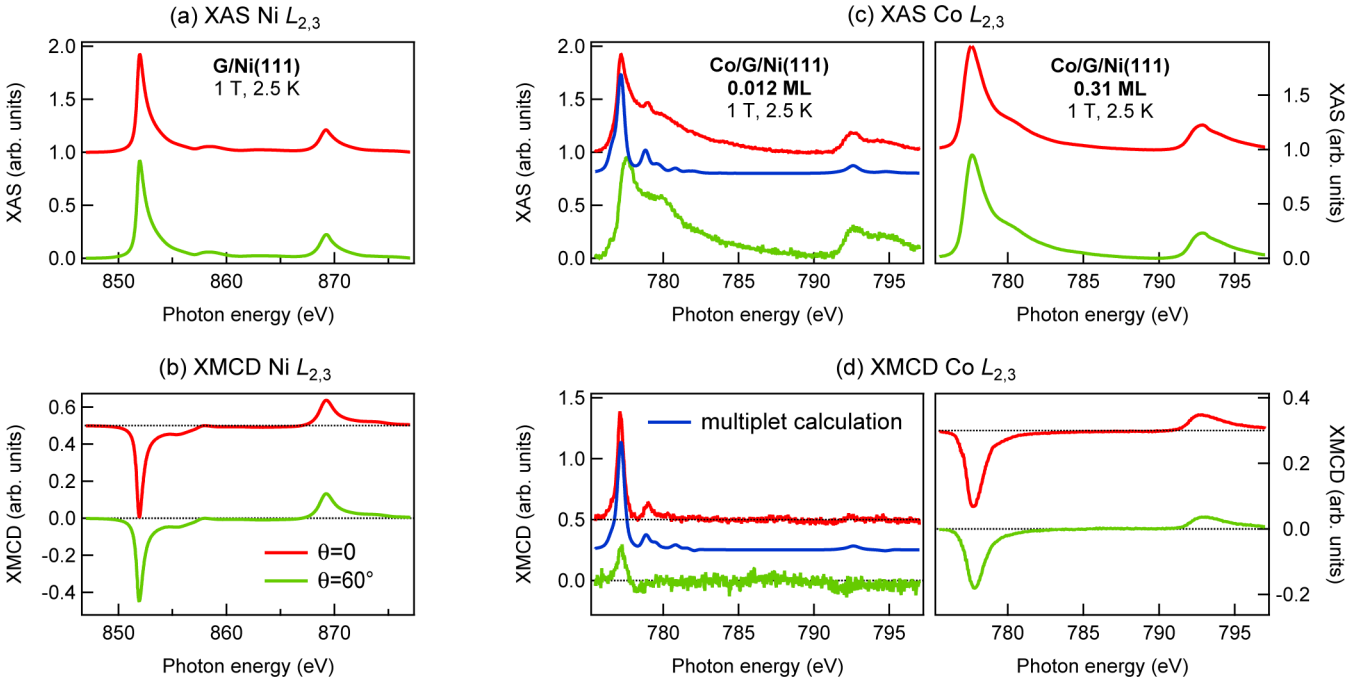

Figure 1. XAS and XMCD recorded at T = 2.5 K and B = 1 T, applied at normal (θ = 0°, red lines) and grazing (θ = 60°, green lines) incidence with respect to the sample surface: (a) XAS and (b) XMCD of G/Ni(111) at the Ni $L_{2,3}$ edges; (c) XAS and (d) XMCD of Co/G/Ni(111) at the Co $L_{2,3}$ edges, for two Co coverages. The XAS and XMCD at normal incidence have been offset for clarity. Multiplet calculations are displayed for normal incidence (blue lines, again offset for clarity).

circular dichroism (XMCD), scanning tunneling microscopy (STM), and density functional theory (DFT), show that single Co atoms adsorb on two different sites with different exchange coupling, while Co atoms with high lateral coordination in small clusters as well as full monolayers (ML) are ferromagnetically coupled with the Ni substrate through the graphene layer.

RESULTS AND DISCUSSION

Electronic and Magnetic Properties. Figure 1 displays the $L_{2,3}$ X-ray absorption (XAS) spectra and the corresponding XMCD of Ni for G/Ni(111) [panels (a) and (b)] and of Co for Co/G/Ni(111) [panels (c) and (d)], at low (0.012 ML) and high (0.31 ML) Co coverage. For the low coverage, where the samples are dominated by individual Co adatoms, the XMCD at the Co L_3 edge is opposite to that of Ni, indicating that the Co magnetization is antiparallel to that of Ni. This shows the existence of a sizable AFM exchange interaction between Co and Ni, mediated by graphene, which dominates the Zeeman energy at the applied field of 1 T. In addition, the magnitude of the Co XMCD is substantially larger when the field is applied perpendicular to the Co/G/Ni(111) surface [see left panel of Figure 1d]. This implies an out-of-plane easy magnetization axis, as previously observed for Co/G/Ru(0001),[25] and is in contrast to the out-of-plane hard axis found for Co/G/Pt(111)[26] and Co/G/Ir(111),[25] or to the almost isotropic behavior of Co/G/SiC(0001).[27] At a coverage of 0.31 ML, the Co XMCD becomes negative [see right panel of Figure 1d], corresponding to a parallel alignment of the Co and Ni magnetizations. In addition, the out-of-plane magnetic anisotropy is strongly reduced, since the difference between in- and out-of-plane spectra diminishes. At intermediate coverages, a coexistence of these two behaviors is observed.

More insight into the electronic configuration of Co adatoms adsorbed onto G/Ni(111) comes from atomic multiplet calculations. The best simulation for the XMCD at 0.012 ML [see left panel of Figure 1d] gives a mixed electronic configuration 28% d^7 + 72% $d^8\underline{L}$ (where $\underline{L}$ is a ligand hole), giving a number of 3d holes n_h = 2.28. The crystal field splits the d-states yielding the $d_{3z^2-r^2}$ orbital as lowest in energy. This configuration was previously reported for Co/G/Ru(0001).[25] It is expected for Co adsorption on top of a carbon atom,[28] and it favors a perpendicular magnetic anisotropy, as observed experimentally. From the multiplet calculations we estimate the expectation values for orbital, spin, and spin dipolar moments at normal incidence: m_L = 2.32 μ_B, m_S = 2.28 μ_B, and m_D = 0.64 μ_B. The corresponding calculated XAS [see left panel in Figure 1c] reproduces the energies of the main multiplet features, although it does not capture all details of the measurement. The remaining broad features, which account for about half of the measured XAS intensity, have no counterpart in the XMCD and can be associated with a fraction of the deposited Co characterized by vanishing magnetization. We observe that this fraction increases over a time scale of 1 h, likely because of beam-induced surface diffusion.

Abundance of Monomers and Dimers at Low Coverage. Low-temperature STM measurements combined with DFT calculations were used to understand the origin of the peculiar features observed in the XAS and XMCD spectra. Figure 2a,c displays low-temperature STM images recorded after Co deposition at 10 K, once at a coverage of 0.0015 ML, where almost solely monomers are present, and once at a coverage of 0.012 ML, identical to the low coverage used in XMCD. Panels (b) and (d) show the statistical analysis of the apparent heights of several hundreds of Co related protrusions. At the lowest coverage, the apparent height histogram shows

DOI: 10.1021/acsnano.5b06410
ACS Nano 2016, 10, 1101−1107

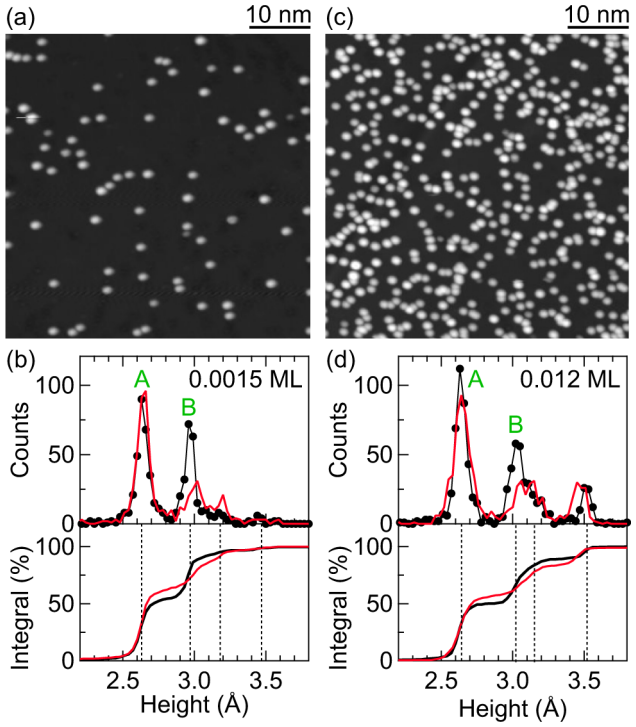

Figure 2. Top panels: STM images of (a) 0.0015 and (c) 0.012 ML Co on G/Ni(111) recorded at T = 4.7 K with V_t = −50 mV, I_t = 20 pA. Bottom panels: Corresponding apparent height histograms (top graph) and integrals (bottom graph). Results obtained immediately after Co deposition at T = 10 K are shown in black and after annealing the sample at T = 20 K for a few minutes in red.

two prominent peaks at 2.63 and 2.95 Å, attributed to species A and B with relative abundance p_A = 54(2)% and p_B = 39(3)%. At 0.012 ML (Figure 2d), these two species occur with slightly decreased abundances p_A = 50(2)% and p_B = 32(3)%. The remaining protrusions at both coverages have higher apparent heights (3.15 and 3.45 Å) and become more abundant with increasing coverage [7(3)% at 0.0015 ML and 18(3)% at 0.012 ML]. Furthermore, heating to only 20 K for a few minutes reduces the relative amount of species B to 25(3) and 13(3)% for Co coverages of 0.0015 and 0.012 ML, respectively (see red curves in Figure 2b,d), with a simultaneous increase of species A and of both species with higher apparent height.

The mean cluster sizes expected from statistical growth on a hexagonal lattice are 1.000 at 0.0015 ML and 1.043 at 0.012 ML.[29] Therefore, only monomers are expected in the first and a few percent of dimers in the second case. From the large abundance of species A and B, and from the observation that heating to 20 K transforms part of species B into A, we attribute A and B to monomers on two adsorption sites, of which B is the metastable one. Annealing also increases the relative amount of the two less abundant species with higher apparent height; thus, we attribute both of them to dimers. Note that the abundance of dimers is significantly larger than expected from statistical growth, indicating transient mobility[30] for the system under study. Regular thermal mobility alone cannot explain our observations since the diffusion rate would have to be significant already at 10 K, meaning that at 20 K it would be so high that on the annealed samples all monomers would disappear in a very short time and form dimers and trimers.

Adsorption Sites and Magnetic Exchange Strength. DFT calculations of a single Co adatom and of a Co monolayer adsorbed on G/Ni(111) were performed. We consider the Co ML as an appropriate representation of our largest islands at 0.31 ML, as it adds the in-plane Co−Co coordination and a Co−Co magnetic exchange to the Co−Ni exchange mediated by graphene. We restrict our discussion to the case of a graphene layer stacked on Ni(111) in the energetically favorable top-fcc geometry,[16,31,32] where one C atom is adsorbed on top of a Ni atom and the other on an fcc hollow site of the Ni(111) surface. We have verified that qualitatively similar conclusions hold also in the case of the energetically less favorable top-bridge stacking geometry (see Supporting Information).

We considered the four possible high-symmetry adsorption sites sketched in Figure 3. We distinguish two sites on top of C,

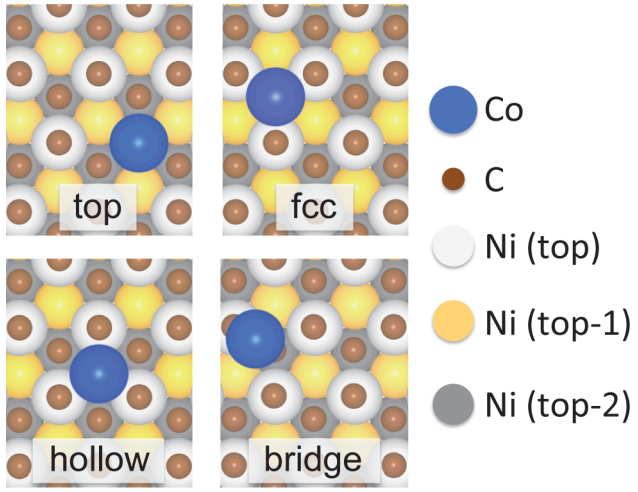

Figure 3. Possible adsorption sites of a Co atom on the G/Ni(111) substrate. The G layer has top-fcc stacking with respect to the Ni(111) surface.

"top" where the C atom below the Co is on a Ni(111) top site and "fcc" where this atom is on an fcc hollow site. The other two sites are the 6-fold G "hollow" and a "bridge" between two C atoms. For each geometry we considered both FM and AFM alignment of Co and Ni spins.

Table 1 shows the total energies of the Co adatom and monolayer on G/Ni(111). In order to account for correlation effects, which were found to be crucial for the magnetic properties of transition metal adatoms on free-standing graphene,[33,34] we used an on-site Hubbard term U = 3 eV[35] and an on-site exchange interaction J = 1 eV. After structural relaxation, we find that the fcc site is the lowest in energy by about 200 meV and has a Co spin moment $m_S \simeq 2.0\ \mu_B$. The hybridization between Co and the substrate is substantial, resulting in a small Co adsorption height of 2.0 Å. Co adatoms on fcc sites have an FM exchange coupling energy to Ni of 4 meV (the magnitude of the magnetic coupling energy is defined as the absolute value of the energy difference between the AFM and the FM configurations). This is in contrast to experiment where a predominantly AFM coupling to Ni is observed. Therefore, we investigated the role of on-site electronic correlations and performed our calculations for Co adatoms also for U > 3 eV (see Table 1). The preferred adsorption site is the fcc site independent of U; however, the exchange coupling energy reverses sign for U > 5 eV where the coupling becomes antiferromagnetic.

DOI: 10.1021/acsnano.5b06410
ACS Nano 2016, 10, 1101−1107

Table 1. Total Energy for a Co Adatom and Monolayer on G/Ni(111)[a]

	top		fcc		hollow		bridge[b]	
	FM	AFM	FM	AFM	FM	AFM	FM	AFM
				Adatom				
U = 3	+226.0	+206.1	**0.0**	+4.2	+317.6	+302.3	-	-
U = 5			**0.0**	+2.5			-	-
U = 7			+2.5	**0.0**			-	-
U = 9	+244.0	+189.9	+5.6	**0.0**	+305.3	+287.5	-	-
				Monolayer				
U = 3	**0.0**	+27.9	+29.7	+25.0	+19.3	+37.8	+16.4	+36.5

[a]As obtained for the indicated U (in eV) and J = 1 eV. The total energy is expressed in meV relative to the ground state (highlighted in bold font). FM (AFM) refers to parallel (antiparallel) alignment of the Co spin moment with respect to the Ni magnetization. [b]The bridge site is not energetically stable in the adatom case and upon structural relaxation the Co adatom moves onto the fcc site.

The top adsorption site, higher in energy by about 200 meV, has large AFM exchange coupling to Ni of 20 meV for U = 3 eV, and this value increases for larger U. The spin moment and the adsorption height are identical to the fcc site.

We also considered Co dimers on G/Ni(111). Similarly to single atoms, Co atoms in dimers prefer to adsorb on adjacent fcc sites for U = 3 eV. Interestingly, we find a Co−Co AFM exchange interaction, which hints at compensated magnetic structures in Co dimers and small clusters,[36,37] suggesting that these contribute only marginally to the XMCD signal and that, at low coverage, mainly the magnetic moment of single Co atoms is probed.[38]

In the case of the Co ML, the preferred adsorption geometry corresponds to Co atoms on top sites, at a distance of 2.9 Å, from the G layer and with a spin moment $m_S \simeq 1.9\ \mu_B$. The magnetic exchange coupling between Co and Ni mediated by graphene is ferromagnetic and in the range of 30 meV/Co-atom.

Magnetic Exchange Coupling Pathways. The adsorption site dependence of the magnetic coupling of Co to the Ni substrate can be related to the geometrical structure and to the Co−C hybridization. Part of the complexity is due to the oscillating spin polarization of the top-fcc stacked graphene layer induced by Ni:[16] C atoms on top of Ni atoms have negative spin polarization ($\simeq -0.02\ \mu_B$) with respect to the Ni sublattice, while C atoms in fcc positions are positively polarized ($\simeq +0.03\ \mu_B$). In fact, Co adatoms, due to the lack of in-plane coordination, have several spin-polarized orbitals that interact with the C atom below as well as with the three neighboring C atoms, which have opposite spin polarization (see Figure 4). Compensation effects take place between the different interaction channels, resulting in a subtle dependence of the exchange coupling on the adsorption site. Thus, single atoms exhibit strong AFM coupling on top and hollow sites, while their coupling is weaker on the fcc sites. Therefore, the experimental observation of an AFM coupling for a fraction of Co atoms that rapidly decreases with increasing temperature (monomers B from the STM investigations) leads to assigning them to top adsorption sites. A hollow site is incompatible with our multiplet calculations and energetically unfavorable with respect to the top sites according to our DFT calculations. Moreover, the calculated Co adsorption height on the hollow sites is by more than 0.3 Å lower than on the fcc sites, in disagreement with the STM observations. Since the adsorption energies for top and fcc sites are strongly different, it is very likely that the diffusion barrier from the metastable to the stable site is very small. Therefore, B monomers can easily diffuse onto fcc sites and thereby become A monomers. This diffusion can either be thermal or X-ray beam-induced.

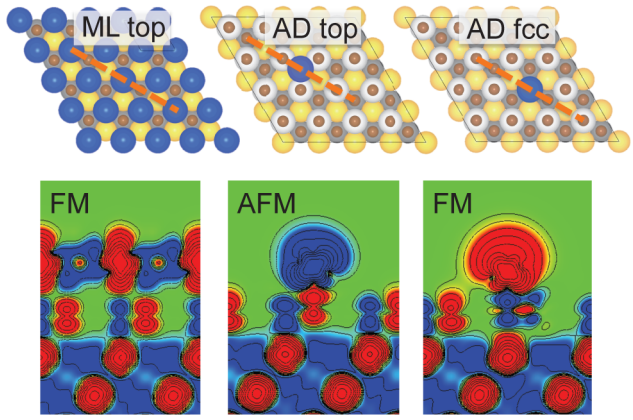

Figure 4. Top: adsorption geometries for Co on G/Ni(111). Bottom: corresponding spin density cross sections (calculated for U = 3 eV) evaluated on a plane cutting through the red dashed line and for the indicated (FM or AFM) relative alignment of Co and Ni spin moments.

Monomers A occupy the most stable fcc site and are more weakly coupled to the Ni magnetization. Their vanishing XMCD may arise from a crystal field scheme leading to a ground state with vanishing projection of the out-of-plane spin component $\langle S_z \rangle = 0$, as previously found for Co/G/Pt(111).[26] Moreover, a local variation of the G−Ni distance due to the small lattice mismatch between G and the Ni(111) surface, with consequent local variations of the electronic screening on the Co d orbitals (corresponding to different values of U in the DFT calculations), can lead to an oscillation of the magnetic coupling between FM and AFM at different fcc sites, whose opposite contributions to the XMCD would, on average, cancel out. Therefore, XMCD is predominantly sensitive to monomers B only, whereas monomers A and dimers give a significant contribution exclusively to the XAS spectra.

For the Co ML, as evident from Figure 4, the spin-polarized $d_{3z^2-r^2}$ orbital of each Co atom interacts only with the π orbital of the adjacent C atom. Thus, the Co spins interact with those of Ni only through the (negative) spin polarization of the nearest C atoms and tend to replicate the spin distribution of the Ni substrate, resulting in a Co−Ni ferromagnetic coupling, as experimentally observed for the 0.31 ML coverage. However, we performed a simulation of a Ni monolayer adsorbed in the same geometry on G/Ni(111) and found that in this case the magnetic coupling is antiferromagnetic. This suggests that other

DOI: 10.1021/acsnano.5b06410
ACS Nano 2016, 10, 1101−1107

parameters, such as the population of the *d* orbitals, play a role in determining the sign of the coupling as well.

Experimental Evaluation of the Magnetic Exchange Coupling Energy. We finally turn to the experimental evaluation of the strength of the magnetic coupling between Co and Ni, mediated by graphene. Figure 5 shows a comparison of the magnetization curves recorded at the Co L_3 edge on Co/G/Ni(111), with those taken at the Ni L_3 edge on G/Ni(111) (in each curve, the magnetization has the sign of the corresponding XMCD). For high coverage (lower panel of Figure 5), Co and Ni are ferromagnetically coupled: their magnetization curves are identical within the statistical accuracy. Without coupling they would saturate at different fields and have different slopes at the origin. At low coverage (upper panel of Figure 5) the cooperative effect of magnetic anisotropy and exchange, both favoring the out-of-plane alignment of the magnetic moments of Co monomers, leads to a saturation of the Co magnetization (opposed to that of Ni) already at 0.1 T, *i.e.*, at lower field than Ni. At the maximum field of 6 T the Co magnetization is still opposed to that of Ni (see inset in the upper panel of Figure 5), thus setting a lower limit of 6 T to the Co−Ni exchange field. This corresponds to an exchange energy of the order of $E_{exch} = -\mu_B(L + 2S)B_{exch} = -1.6$ meV, where $L = 2.32$ and $2S = 2.28$ are the orbital and spin angular momenta of Co monomers determined from the multiplet calculations.

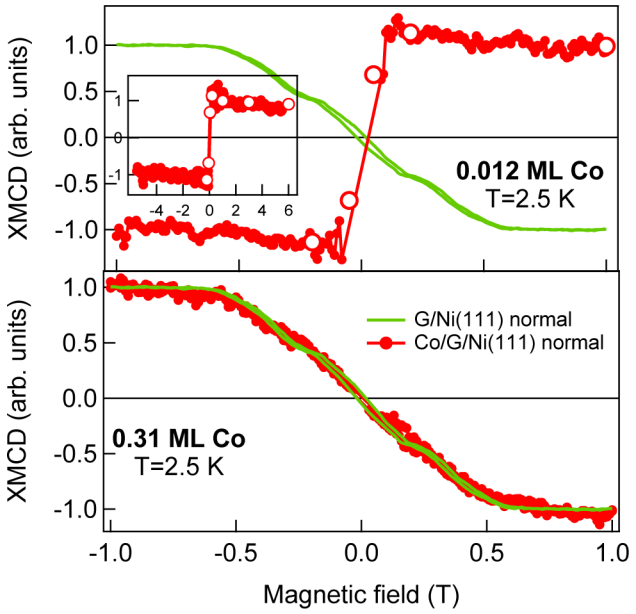

Figure 5. Magnetization curves recorded, at normal incidence, at the Ni L_3 edge on G/Ni(111) (full green lines) and at the Co L_3 edge on Co/G/Ni(111) (filled red circles), at a temperature of about 2.5 K. The inset of the top panel shows the full curve up to a field of 6 T for the low coverage. Open symbols in the top panel indicate XMCD data extracted from full XAS scans as those shown in Figure 1.

CONCLUSIONS

In conclusion, we observe an adsorption-site dependent, predominantly AFM exchange coupling between individual Co atoms and Ni(111) mediated by an epitaxial graphene layer. In addition, the Co adatoms have a strong out-of-plane magnetic anisotropy. The coupling changes sign and becomes FM as the Co coverage is increased up to the monolayer range. Our results underline the sensitivity of the exchange interaction across graphene to the local coordination and to the geometrical arrangement of the magnetic layers. These findings are important for the utilization of graphene as a spacer layer in magnetic heterostructures and spintronic devices, as well as to understand the complex interaction between graphene and magnetic impurities.

METHODS

The Ni(111) single crystal was prepared by repeated cycles of Ar^+ sputtering and annealing at a temperature of about 1050 K. Graphene monolayers were grown by thermal decomposition of ethylene at 950 K (9000 L). For the XAS experiments, Co was evaporated *in situ* onto G/Ni(111) at $T < 5$ K and $p \approx 3 \times 10^{-11}$ mbar. In order to calibrate the Co coverage, a small amount of Co (in the submonolayer range) was evaporated onto the clean Ni(111) surface at $T < 5$ K, and its X-ray absorption spectrum was recorded. After heating to 300 K, flat Co islands form, and the fraction of the Ni(111) surface covered by Co is determined by STM. This establishes a direct link between the Co coverage and the XAS signal. For the STM experiments, cobalt atoms were deposited using an e-beam evaporator on the sample positioned in the STM at $T = 10$ K. The Co atom flux was calibrated at low coverage by measuring the density of monomers. Coverages are given in monolayers (ML), where one ML is defined as one Co atom per substrate (Ni) atom.

The XMCD experiments were carried out at the EPFL/PSI X-Treme beamline[39] of the Swiss Light Source. The measurements were performed in the total-electron-yield mode at a temperature of about 2.5 K, and magnetic fields up to 6 T were applied parallel to the X-ray beam. After recording the X-ray absorption spectra of both G/Ni(111), prior to Co evaporation, and Co/G/Ni(111) at the Co $L_{2,3}$ edges under identical conditions, the Co XMCD is extracted as follows: The average background subtracted XAS $[(I^+ + I^-)/2$, where I^+ and I^- are the XAS spectra recorded with right and left circularly polarized X-rays, respectively$]$ has been normalized to unity at the most intense peak of the L_3 edge, prior to subtraction of step functions at the two edges, and the XMCD is calculated as $I^- - I^+$.

Charge-transfer atomic multiplet calculations were performed using the CTM4XAS code.[40] We used the values $10Dq = 0$, $Ds = 0.333$ eV, and $Dt = 0.2$ eV to describe the uniaxial crystal field. Charge transfer was simulated with an energy $\Delta = -2.5$ eV, a core−hole interaction $U_{p-d} - U_{d-d} = 1.1$ eV, and hopping integrals $t(a1) = 0.8$ eV, $t(e1) = 0.5$ eV, and $t(e2) = 0.25$ eV. The Slater−Condon integrals have been rescaled to 72% to account for the chemical bonding.

The STM measurements were performed with a homemade microscope operating at 4.7 K.[41] We used W tips for all measurements, and the images were acquired in constant current mode (the indicated tunnel voltages correspond to the sample potential).

The DFT calculations were carried out using the Vienna *ab initio* simulation package (VASP),[42,43] where GGA-PAW pseudopotentials were employed, together with empirical vdW dispersion terms[44] and Hubbard-type + U corrections.[35] We simulated G/Ni(111) using a 4-ML-thick Ni slab with one graphene layer adsorbed on one side. About 25 Å of vacuum space is inserted to avoid spurious interactions between the slab replicas. Calculations of the Co monolayer have been carried out using the (1×1) in-plane unit cell composed of 1 Co, 2 C, and 1 Ni atoms in each layer and a 20×20 *k*-point grid. A (4×4) in-plane unit cell containing 32 C and 16 Ni atoms/layer and a 8×8 *k*-point grid have been employed for the adatom and dimer calculations. Structural relaxations have been performed for the Co atoms, the graphene, and the topmost Ni layer, until remanent forces were smaller than 0.02 eV $Å^{-1}$. PAW−PBE pseudopotentials with a cutoff energy of 500 eV for the plane wave basis set and a kinetic energy cutoff of 700 eV for the augmentation charges have been used.

DOI: 10.1021/acsnano.5b06410
ACS Nano 2016, 10, 1101−1107

ASSOCIATED CONTENT

Supporting Information

The Supporting Information is available free of charge on the ACS Publications website at DOI: 10.1021/acsnano.5b06410.

Complete coverage dependence of the Co XMCD, XAS and XMCD measurements on Co/Ni(111), and calculated exchange coupling for the bridge-top stacking of graphene on the Ni(111) surface (PDF)

AUTHOR INFORMATION

Corresponding Author

*(A.B.) E-mail: alessandro.barla@trieste.ism.cnr.it.

Notes

The authors declare no competing financial interest.

ACKNOWLEDGMENTS

This work has been funded by the European Community's Seventh Framework Programme (FP7/2007-2013) under Grant Agreement No. 312284 (CALIPSO), the SFB 677 project, the Swiss National Science Foundation (Grant No. 200021-153404), and MIUR (FIRB-Futuro in Ricerca 2010, Project PLASMOGRAPH, Grant No. RBFR10M5BT, and Progetto Premiale "Materiali e disposivi magnetici e superconduttivi per sensoristica e ICT"). L.P. acknowledges support from the ETHZ Postdoctoral Fellowship Program. Computation time at HLRN and CINECA supercomputing centers is also gratefully acknowledged. The X-ray absorption measurements were performed on the EPFL/PSI X-Treme beamline at the Swiss Light Source, Paul Scherrer Institut, Villigen, Switzerland.

REFERENCES

(1) Novoselov, K. S.; Geim, A. K.; Morozov, S. V.; Jiang, D.; Zhang, Y.; Dubonos, S. V.; Grigorieva, I. V.; Firsov, A. A. Electric Field Effect in Atomically Thin Carbon Films. *Science* **2004**, *306*, 666−669.

(2) Zhang, Y.; Tan, Y.-W.; Stormer, H. L.; Kim, P. Experimental Observation of the Quantum Hall Effect and Berry's Phase in Graphene. *Nature* **2005**, *438*, 201−204.

(3) Tombros, N.; Jozsa, C.; Popinciuc, M.; Jonkman, H. T.; van Wees, B. J. Electronic Spin Transport and Spin Precession in Single Graphene Layers at Room Temperature. *Nature* **2007**, *448*, 571−574.

(4) Han, W.; Kawakami, R. K. Spin Relaxation in Single-Layer and Bilayer Graphene. *Phys. Rev. Lett.* **2011**, *107*, 047207.

(5) Dlubak, B.; Martin, M.-B.; Deranlot, C.; Servet, B.; Xavier, S.; Mattana, R.; Sprinkle, M.; Berger, C.; De Heer, W. A.; Petroff, F.; et al. Highly Efficient Spin Transport in Epitaxial Graphene on SiC. *Nat. Phys.* **2012**, *8*, 557−561.

(6) Kim, D.; Hashmi, A.; Hwang, C.; Hong, J. Magnetization Reversal and Spintronics of Ni/Graphene/Co Induced by Doped Graphene. *Appl. Phys. Lett.* **2013**, *102*, 112403.

(7) Garcia-Lekue, A.; Balashov, T.; Ollé, M.; Ceballos, G.; Arnau, A.; Gambardella, P.; Sanchez-Portal, D.; Mugarza, A. Spin-Dependent Electron Scattering at Graphene Edges on Ni(111). *Phys. Rev. Lett.* **2014**, *112*, 066802.

(8) Olsen, T.; Yan, J.; Mortensen, J. J.; Thygesen, K. S. Dispersive and Covalent Interactions between Graphene and Metal Surfaces from the Random Phase Approximation. *Phys. Rev. Lett.* **2011**, *107*, 156401.

(9) Mittendorfer, F.; Garhofer, A.; Redinger, J.; Klimeš, J.; Harl, J.; Kresse, G. Graphene on Ni(111): Strong Interaction and Weak Adsorption. *Phys. Rev. B: Condens. Matter Mater. Phys.* **2011**, *84*, 201401.

(10) Karpan, V. M.; Giovannetti, G.; Khomyakov, P. A.; Talanana, M.; Starikov, A. A.; Zwierzycki, M.; van den Brink, J.; Brocks, G.; Kelly, P. J. Graphite and Graphene as Perfect Spin Filters. *Phys. Rev. Lett.* **2007**, *99*, 176602.

(11) Karpan, V. M.; Khomyakov, P. A.; Starikov, A. A.; Giovannetti, G.; Zwierzycki, M.; Talanana, M.; Brocks, G.; van den Brink, J.; Kelly, P. J. Theoretical Prediction of Perfect Spin Filtering at Interfaces between Close-Packed Surfaces of Ni or Co and Graphite or Graphene. *Phys. Rev. B: Condens. Matter Mater. Phys.* **2008**, *78*, 195419.

(12) Yazyev, O. V.; Pasquarello, A. Magnetoresistive Junctions Based on Epitaxial Graphene and Hexagonal Boron Nitride. *Phys. Rev. B: Condens. Matter Mater. Phys.* **2009**, *80*, 035408.

(13) Cobas, E.; Friedman, A. L.; van't Erve, O. M. J.; Robinson, J. T.; Jonker, B. T. Graphene As a Tunnel Barrier: Graphene-Based Magnetic Tunnel Junctions. *Nano Lett.* **2012**, *12*, 3000−3004.

(14) Hermanns, C. F.; Tarafder, K.; Bernien, M.; Krüger, A.; Chang, Y.-M.; Oppeneer, P. M.; Kuch, W. Magnetic Coupling of Porphyrin Molecules Through Graphene. *Adv. Mater.* **2013**, *25*, 3473−3477.

(15) Bhandary, S.; Eriksson, O.; Sanyal, B. Defect Controlled Magnetism in FeP/Graphene/Ni(111). *Sci. Rep.* **2013**, *3*, 3405.

(16) Marocchi, S.; Ferriani, P.; Caffrey, N. M.; Manghi, F.; Heinze, S.; Bellini, V. Graphene-Mediated Exchange Coupling between a Molecular Spin and Magnetic Substrates. *Phys. Rev. B: Condens. Matter Mater. Phys.* **2013**, *88*, 144407.

(17) Klar, D.; Bhandary, S.; Candini, A.; Joly, L.; Ohresser, P.; Klyatskaya, S.; Schleberger, M.; Ruben, M.; Affronte, M.; Eriksson, O.; et al. Field-Regulated Switching of the Magnetization of Co-Porphyrin on Graphene. *Phys. Rev. B: Condens. Matter Mater. Phys.* **2014**, *89*, 144411.

(18) Candini, A.; Bellini, V.; Klar, D.; Corradini, V.; Biagi, R.; De Renzi, V.; Kummer, K.; Brookes, N. B.; del Pennino, U.; Wende, H.; et al. Ferromagnetic Exchange Coupling between Fe Phthalocyanine and Ni(111) Surface Mediated by the Extended States of Graphene. *J. Phys. Chem. C* **2014**, *118*, 17670−17676.

(19) Gambardella, P.; Rusponi, S.; Veronese, M.; Dhesi, S. S.; Grazioli, C.; Dallmeyer, A.; Cabria, I.; Zeller, R.; Dederichs, P. H.; Kern, K.; et al. Giant Magnetic Anisotropy of Single Cobalt Atoms and Nanoparticles. *Science* **2003**, *300*, 1130−1133.

(20) Rusponi, S.; Cren, T.; Weiss, N.; Epple, M.; Buluschek, P.; Claude, L.; Brune, H. The Remarkable Difference Between Surface and Step Atoms in the Magnetic Anisotropy of Two-Dimensional Nanostructures. *Nat. Mater.* **2003**, *2*, 546−551.

(21) Krause, S.; Herzog, G.; Stapelfeldt, T.; Berbil-Bautista, L.; Bode, M.; Vedmedenko, E. Y.; Wiesendanger, R. Magnetization Reversal of Nanoscale Islands: How Size and Shape Affect the Arrhenius Prefactor. *Phys. Rev. Lett.* **2009**, *103*, 127202.

(22) Rohart, S.; Campiglio, P.; Repain, V.; Nahas, Y.; Chacon, C.; Girard, Y.; Lagoute, J.; Thiaville, A.; Rousset, S. Spin-Wave-Assisted Thermal Reversal of Epitaxial Perpendicular Magnetic Nanodots. *Phys. Rev. Lett.* **2010**, *104*, 137202.

(23) Ouazi, S.; Vlaic, S.; Rusponi, S.; Moulas, G.; Buluschek, P.; Halleux, K.; Bornemann, S.; Mankovsky, S.; Minár, J.; Staunton, J. B.; et al. Atomic-Scale Engineering of Magnetic Anisotropy of Nanostructures through Interfaces and Interlines. *Nat. Commun.* **2012**, *3*, 1313.

(24) Ouazi, S.; Wedekind, S.; Rodary, G.; Oka, H.; Sander, D.; Kirschner, J. Magnetization Reversal of Individual Co Nanoislands. *Phys. Rev. Lett.* **2012**, *108*, 107206.

(25) Donati, F.; Gragnaniello, L.; Cavallin, A.; Natterer, F.; Dubout, Q.; Pivetta, M.; Patthey, F.; Dreiser, J.; Piamonteze, C.; Rusponi, S.; et al. Tailoring the Magnetism of Co Atoms on Graphene through Substrate Hybridization. *Phys. Rev. Lett.* **2014**, *113*, 177201.

(26) Donati, F.; Dubout, Q.; Autès, G.; Patthey, F.; Calleja, F.; Gambardella, P.; Yazyev, O. V.; Brune, H. Magnetic Moment and Anisotropy of Individual Co Atoms on Graphene. *Phys. Rev. Lett.* **2013**, *111*, 236801.

(27) Eelbo, T.; Waśniowska, M.; Thakur, P.; Gyamfi, M.; Sachs, B.; Wehling, T. O.; Forti, S.; Starke, U.; Tieg, C.; Lichtenstein, A. I.; et al. Adatoms and Clusters of 3*d* Transition Metals on Graphene: Electronic and Magnetic Configurations. *Phys. Rev. Lett.* **2013**, *110*, 136804.

(28) Wehling, T. O.; Balatsky, A. V.; Katsnelson, M. I.; Lichtenstein, A. I.; Rosch, A. Orbitally Controlled Kondo Effect of Co Adatoms on Graphene. *Phys. Rev. B: Condens. Matter Mater. Phys.* **2010**, *81*, 115427.
(29) Brune, H. Microscopic View of Epitaxial Metal Growth: Nucleation and Aggregation. *Surf. Sci. Rep.* **1998**, *31*, 125−229.
(30) Brune, H. In *Handbook of Surface Science*; Lundqvist, B. I., Hasselbrink, E., Eds.; Dynamics: North-Holland, 2008; Vol. *3*; pp 761−786.
(31) Bianchini, F.; Patera, L. L.; Peressi, M.; Africh, C.; Comelli, G. Atomic Scale Identification of Coexisting Graphene Structures on Ni(111). *J. Phys. Chem. Lett.* **2014**, *5*, 467−473.
(32) Garcia-Lekue, A.; Ollé, M.; Sanchez-Portal, D.; Palacios, J. J.; Mugarza, A.; Ceballos, G.; Gambardella, P. Substrate-Induced Stabilization and Reconstruction of Zigzag Edges in Graphene Nanoislands on Ni(111). *J. Phys. Chem. C* **2015**, *119*, 4072−4078.
(33) Wehling, T. O.; Lichtenstein, A. I.; Katsnelson, M. I. Transition-Metal Adatoms on Graphene: Influence of Local Coulomb Interactions on Chemical Bonding and Magnetic Moments. *Phys. Rev. B: Condens. Matter Mater. Phys.* **2011**, *84*, 235110.
(34) Rudenko, A. N.; Keil, F. J.; Katsnelson, M. I.; Lichtenstein, A. I. Adsorption of Cobalt on Graphene: Electron Correlation Effects from a Quantum Chemical Perspective. *Phys. Rev. B: Condens. Matter Mater. Phys.* **2012**, *86*, 075422.
(35) Liechtenstein, A. I.; Anisimov, V. I.; Zaanen, J. Density-Functional Theory and Strong Interactions: Orbital Ordering in Mott-Hubbard Insulators. *Phys. Rev. B: Condens. Matter Mater. Phys.* **1995**, *52*, R5467−R5470.
(36) Lounis, S.; Mavropoulos, P.; Dederichs, P. H.; Blügel, S. Noncollinear Korringa-Kohn-Rostoker Green Function Method: Application to 3*d* Nanostructures on Ni(001). *Phys. Rev. B: Condens. Matter Mater. Phys.* **2005**, *72*, 224437.
(37) Otte, F.; Ferriani, P.; Heinze, S. Complex Trend of Magnetic Order in Fe Clusters on 4*d* Transition-Metal Surfaces. II. First-Principles Calculations. *Phys. Rev. B: Condens. Matter Mater. Phys.* **2014**, *89*, 205426.
(38) Sessi, V.; Otte, F.; Krotzky, S.; Tieg, C.; Wasniowska, M.; Ferriani, P.; Heinze, S.; Honolka, J.; Kern, K. Complex Trend of Magnetic Order in Fe Clusters on 4*d* Transition-Metal Surfaces. I. Experimental Evidence and Monte Carlo Simulations. *Phys. Rev. B: Condens. Matter Mater. Phys.* **2014**, *89*, 205425.
(39) Piamonteze, C.; Flechsig, U.; Rusponi, S.; Dreiser, J.; Heidler, J.; Schmidt, M.; Wetter, R.; Calvi, M.; Schmidt, T.; Pruchova, H.; et al. X-Treme Beamline at SLS: X-Ray Magnetic Circular and Linear Dichroism at High Field and Low Temperature. *J. Synchrotron Radiat.* **2012**, *19*, 661−674.
(40) Stavitski, E.; de Groot, F. M. F. The CTM4XAS Program for EELS and XAS Spectral Shape Analysis of Transition Metal L Edges. *Micron* **2010**, *41*, 687−694.
(41) Gaisch, R.; Gimzewski, J. K.; Reihl, B.; Schlittler, R. R.; Tschudy, M.; Schneider, W. D. Low-Temperature Ultra-High-Vacuum Scanning Tunneling Microscope. *Ultramicroscopy* **1992**, *42*−*44*, 1621−1626.
(42) Kresse, G.; Furthmüller, J. Efficient Iterative Schemes for *Ab Initio* Total-Energy Calculations Using a Plane-Wave Basis Set. *Phys. Rev. B: Condens. Matter Mater. Phys.* **1996**, *54*, 11169−11186.
(43) Kresse, G.; Joubert, D. From Ultrasoft Pseudopotentials to the Projector Augmented-Wave Method. *Phys. Rev. B: Condens. Matter Mater. Phys.* **1999**, *59*, 1758−1775.
(44) Grimme, S. Semiempirical GGA-Type Density Functional Constructed with a Long-Range Dispersion Correction. *J. Comput. Chem.* **2006**, *27*, 1787−1799.

DOI: 10.1021/acsnano.5b06410
ACS Nano 2016, 10, 1101−1107